Thermodynamic study of the ^{4}He monolayer adsorbed on Grafoil*

Robert L. Elgin† and David L. Goodstein
Department of Physics, California Institute of Technology, Pasadena, California 91109
(Received 17 December 1973)

A calorimetric and vapor-pressure study of the behavior of ^{4}He adsorbed on Grafoil in the temperature range 4 to 15 K is reported. These results have been combined with preexisting low-temperature heat-capacity data to form a complete thermodynamic description of the film. The Grafoil substrate evidently consists almost entirely of basal-plane graphite, with only a small fraction of energetically distinct adsorption sites. Techniques of semiempirical modelling are introduced which make it possible to eliminate the effects both of these inhomogeneities and of the formation of second and higher layers, so that a detailed picture may be formed of the behavior of the ^{4}He first layer on an ideal graphite substrate. The binding energy of a ^{4}He atom on the graphite substrate is reported to be 143 ± 2 K, with a first excited state at 89 ± 3 K. A lattice-gas ordering transition occurs near 3 K at a coverage corresponding to one ^{4}He atom for every three carbon hexagons in the graphite surface, and is used as a fiducial for calibrating our system relative to those of previous investigators. At both higher and lower densities the film seems little influenced by the crystal structure of the substrate. Particular attention is given to the high-coverage low-temperature region, which has been identified as a two-dimensional (2D) solid bounded by a melting-phase transition. The available data are combined with two-dimensional elastic theory to establish the presence of low-lying transverse sound modes, thus confirming the solidlike character of this medium. The behavior of the thermodynamic variables of state through the observed transition is also presented. The theoretical implications of the existence of a 2D solid are discussed, together with a dislocation theory of melting which gives rise to the well-known three-dimensional Lindemann empirical melting formula without an adjustable parameter. It is shown that at very low coverage the film does not form a low-density solid as previously suggested, but is rather dominated by substrate inhomogeneities. At intermediate temperatures and coverages the film is a fluid which is accurately described if a leading-order quantum virial correction is made to the 2D ideal-gas equation of state.

I. INTRODUCTION

In a recent paper, Bretz, Dash, Hickernell, McLean, and Vilches,[1] hereafter known as BDHMV, presented a survey of the behavior of thin helium films adsorbed on a graphite substrate called Grafoil.[2] In this paper we present extensive new data on the system ^{4}He on Grafoil and detailed analysis, both thermodynamic and model-based, in an attempt to answer some of the experimental and theoretical questions that have arisen in connection with these systems. The importance of these systems lies in the fact that the adsorbate behaves in many respects as if it were constrained to move in an ideal plane. The results thus allow an experimental comparison between the properties of matter in two dimensions (2D) and in three dimensions (3D).

The BDHMV experiments were principally measurements of the relatively low temperature heat capacities of the He-Grafoil system. The new data reported in the present paper, hereafter referred to as the Caltech data, are principally concentrated at higher temperatures (4 to 15 K) and include both vapor-pressure and calorimetric measurements. As explained in Sec. III, both kinds of data are required for a complete thermodynamic characterization of the system.

The Caltech and BDHMV data may be compared where they overlap, using the "ordering peak" as a fiducial for calibrating surfaces in the two laboratories, as explained in Sec. IV. Although some uncertainties are found to exist, the over-all result of intercomparison of the data is a striking confirmation of the reproducibility of both the qualitative and quantitative features observed. Internal comparisons are given in Sec. IV between Caltech data from vapor-pressure measurements and from heat-capacity measurements in regions where those two techniques are redundant. Good agreement is found.

As explained in Sec. III, the Caltech data may be used in combination with BDHMV to generate a complete thermodynamic characterization in the regions of temperature and pressure covered by either portion of the combined data. For example, from a tabulation of the Landau potential Ω as a function of temperature T and chemical potential μ, one can obtain all other thermodynamic quantities by taking appropriate derivatives. Having such detailed thermodynamic information in hand, we have been able to analyze the phenomena observed in this system in ways which have not previously been possible. One example is

that we have been able quite accurately to find from these measurements the gas pressure in equilibrium with the film at pressures much too low to have been measured by conventional means. For instance, we report a pressure of 1.4×10^{-17} torr for the "ordering peak." Moreover, the results of our thermodynamic analysis allow us to make direct tests of a number of theoretical models proposed for various aspects of the ^{4}He-Grafoil system. These theories and their comparison with the data are discussed where appropriate in Secs. V–VII.

In both the low-coverage region and at coverages near one layer, we have worked out simple, semiempirical models which, we believe, both greatly facilitate handling of the data by providing analytic equations of state to work with, and also allow us to understand quantitatively, and to separate out, the effects of inhomogeneity at low coverage, and of second-layer formation at high coverage. These models are presented and discussed in Sec. V. Sections VI and VII are devoted to discussions of the states of 2D matter found, respectively, at high density (in the vicinity of monolayer coverage) and low density (below the ordering peak).

On the basis of their heat-capacity data, BDHMV have proposed a phase diagram for the He-Grafoil system in the coverage-temperature plane, assigning identifications to some of the phases and apparent phase transitions observed. We shall present evidence tending to corroborate their identifications in two particularly important instances: the solid phase and the melting transition. In the case of the solid phase, available data together with two-dimensional elastic theory may be used to argue that the region identified as solid has the solidlike property of resisting shear stresses and supporting transverse sound modes. We also show that the relations between two-dimensional pressure, density, and temperature, in the vicinity of what BDHMV call the melting curve, are indeed reminiscent of melting in the bulk, with the important exception that the transition in the film is not first order. The apparent existence of a solid phase and melting transition in the ^{4}He-Grafoil system calls into question current ideas concerning the nonexistence of long-range order in 2D. These ideas are considered in the light of the data in Sec. VI, and a recent theory of melting in 2D is discussed. We find ourselves in disagreement with the BDHMV assignment to the low-coverage region of a low-density solid. Instead, the same data are accounted for in detail by the simple modeling of the effect of observed substrate inhomogeneity mentioned above.

The contents of the sections are as follows: Sec. I, Introduction; Sec. II, Experimental Apparatus and Technique, including a discussion of the criteria for equilibrium in experiments of this kind; Sec. III, Thermodynamic Analysis; Sec. IV, Data; Sec. V, Modeling the Film; Sec. VI, Solid State and Melting Transition; Sec. VII, Ordering Peak and Lower Densities; and Sec. VIII, Conclusions.

II. EXPERIMENTAL APPARATUS AND TECHNIQUE

A. Equipment

Some of the ensuing manipulations may be esoteric but the experimental apparatus and methods are straightforward. The apparatus consists of a pile of Grafoil sheets in a copper cell suspended in a vacuum chamber surrounded by a liquid-helium bath. Temperature is measured and regulated by means of a germanium thermometer and an Evanohm wire heater on the outside of the cell. Metered amounts of helium are let into the cell through a filling line that also allows the pressure to be measured by a capacitive manometer at room temperature.

The Grafoil came in a nominally 0.38-mm thick sheet. It was cut into 55 disks, 2.86 cm in diameter. Four 3.2-mm holes and 24 radial slits were cut into each disk to improve gas flow. The result weighed 12.51 g after baking in vacuo at 900 °C for 1 h. After interleaving with 27 sheets of 0.05-mm shim copper to improve the thermal conductivity, the disks were gently pressed into a copper cell. A copper base was silver soldered on in a hydrogen atmosphere and the resulting cell was then soft soldered onto the 1.56-mm-i.d. CuNi filling line and baked above 100 °C under vacuum for a week. General Electric-type 7031 varnish was used to apply the 480-Ω heater wire. The germanium thermometer was screwed into the top and the leads varnished to the cell for better thermal contact. The complete calorimeter consists of 14 g of Grafoil (partly in an unused secondary cell), 64 g of copper, 3 g of other metals, and less than 0.2 g of other materials. The free volume is 9.5 cm^3.

Manganin wires, thermally grounded to the vacuum chamber, form leads to the heater and thermometer. The filling line is baffled and loosely coupled to the chamber so that it is about 0.5-K warmer than the helium bath at its coldest point. A 0.64-cm-i.d. monel tube filled with low-pressure helium gas and containing a copper plunger was used to vary the thermal contact between the calorimeter and the bath.[3]

The gas-handling system consists of a number of calibrated volumes, two capacitive manometers, and pumps. The germanium resistance was mea-

sured by use of a Wheatstone bridge and a lock-in amplifier. The temperature was regulated by manually adjusting the output of a variable-voltage power supply. The heat-capacity heat pulses were generated by the same method.[4]

B. Calibrations

The calibrated volumes, their temperature, and the pressure could all be measured to better than 0.1%. The pressure of the gas added to the system was always less than 500 torr, so the gas was ideal to better than 0.1%. The gas purity was checked at the end of the run by measuring the fraction of the gas that could not be removed by pumping at 70 K. This was generally less than 0.01%, but for the early data a leak in the storage volume raised it to 0.12%. This has been subtracted from the affected data so the amount of helium in the cell is always known to 0.1%.

The germanium thermometer was calibrated against the vapor pressure of ^{4}He from 1.5 to 3.5 K and against a constant volume gas thermometer from 4 to 25 K. Interpolation and smoothing was done using the heat capacity of a copper sample. The largest source of error appears to have been variations in resistance in the leads and the Wheatstone bridge. The temperature scale is believed to be accurate to 0.2% and the derivative used in the heat-capacity measurements to 0.5%.

As already mentioned, the pressure at room temperature could be measured to better than 0.1% down to 0.02 torr. Unfortunately, differences of opinion in the literature[5] on the size of the thermal transpiration correction are as much as a factor of 2 in the millitorr region. To overcome this problem we calibrated the transpiration correction *in situ* by the absolute method, replacing the adsorption cell by a large, empty cell and by comparing with the pressures calculated from the heat capacity where the film data are redundant. The calibration curve was fit by an empirical modification of the equation of Weber and Schmidt.[6] We believe the calculated pressures at the cell to be accurate to 0.1% above 2 torr, to 1% above 0.3 torr, and to 3% above 0.2 mtorr.

The resistance of the heater wire at low temperature was only known to 0.2% but was constant to much higher accuracy. The current and time of the heat pulses were easily measured to 0.02%. The main source of error in the heat capacity was caused by uncertainty in how much of the added heat actually warmed the helium film.

Of the heat added to the calorimeter, part is lost to heat leaks, part warms up the copper and Grafoil container, part warms the helium gas, part causes the film to desorb, and part warms the film. The first two terms were evaluated very accurately as a unit, by using the same temperature intervals and same temperature rise rate with and without helium in the cell. Since the (OFHC copper) outer surface of the calorimeter is a very good heat conductor, the heat flows to the outside world under these conditions are independent of the coverage (except for a slight cooling of the filling line by desorbing gas at high pressures). The heat capacity of the helium gas in the cell is easily calculated since the pressure is measured directly. The desorption correction will be derived rigorously in Sec. III from the temperature variation of the pressure at constant coverage. The accuracy of the remaining film heat capacity varies greatly because it is the remainder after subtracting all the other terms. Over most of the data range it is comparable to the 0.5% accuracy of the derivative of the temperature calibration, but below one-tenth of a layer and above 10 torr in pressure the uncertainties rise as high as 5%.

The actual amount of helium adsorbed on the Grafoil (the coverage) can be found by subtracting the helium in the gas state from the total in the system, since the sum of all other surfaces is negligible. Only the bottom 7.5 cm of the filling line was near helium temperatures and this contributes 0.2 cm^3 to the cold volume in addition to the 9.5 cm^3 of the calorimeter proper. The remainder of the filling line and the tubing connecting the capacitive manometers was equivalent to 47 cm^3 at room temperature. Since large uncertainties in the cell pressure occur only when this correction is small, the amount of helium adsorbed is known to the 0.1% accuracy of the total gas added except in the multilayer, high-temperature region.

C. Equilibrium

Accurate data are of little use in a thermodynamic analysis unless the sample is in equilibrium. For complete equilibrium, the temperature and the chemical potential must be the same for all helium atoms in the calorimeter. A nonuniform temperature distribution could easily be detected by the variation in the apparent heat leak while the thermometric temperature was held constant. This always disappeared within a few minutes. A nonuniform chemical potential distribution was detected by the drift in the pressure when this was large enough to be measured easily. At low temperatures the lack of a measurable pressure removes both the best means of obtaining chemical potential equilibrium and the best method of verifying it. We therefore had to develop a method of preparation for the low-temperature film that assured this equilibrium *a priori*.

A common procedure for improving the uni-

formity of adsorbed films is to anneal them at "high" temperature. This unfortunately gives only negative information: if the film changes, then at least one set of data was not at equilibrium. For a positive indication, we used a pressure criterion. In general, if a submonolayer film formed at low temperature was warmed just to the point at which the manometry reached full accuracy (0.01 torr), drifts were observed for a day or longer. At higher temperatures the drift time fell at least in proportion to the increase in pressure, reaching a few minutes at 10 torr. At this point we had complete equilibrium, but helium equivalent of up to 2% of a monolayer was in the gas state. If the cell were cooled rapidly, most of this gas would condense on the nearest cold surface, re-creating a nonequilibrium film. On the other hand, if the cell is cooled slowly, the mass to be redistributed drops proportionally with the pressure so that the relaxation time should remain almost constant. This was observed to be the case. When the temperature was reduced at the rate of 1% per minute and then stabilized, the pressure also stabilized within the next 10 minutes, whether it was near 1 torr or near 0.01 torr. The procedure probably continues to work to much lower pressures, but that is not important because at the latter pressure only 0.002% of a monolayer remains in the gas state. (Similar behavior was not obtained when cooling more rapidly than 2% in temperature per minute; instead, the stabilization time grew without limit as the temperature decreased.) It should be noted that this technique is conservative since a very small amount of helium condensed at the base of the filling line may have a large effect on the pressure without significantly affecting the heat capacity.

Since we were interested in both the pressure and the heat capacity, the temperature was lowered in 10% decrements each followed by 10 minute periods during which the pressure reached equilibrium and was recorded. The heat capacity could then be taken over 10% increments in temperature followed by only 4 minute waiting periods because a given deviation from equilibrium becomes rapidly annealed on further heating as contrasted to becoming frozen in on further cooling.

The initial temperatures needed for this technique varied considerably with coverage. For a freshly formed film of 0.01, 0.1, 0.5, and 1.0 monolayer the temperatures needed were 17, 16, 14, and 7 K, respectively. For 10% increments in coverage to previously annealed films, about 20% lower temperatures were sufficient. Assuming that the mass flow rate continues to be proportional to the pressure at much lower pressures, the more conventional technique of annealing overnight at a constant temperature should work if that temperature is above 11, 10, 9, and 3.5 K, respectively.

III. THERMODYNAMIC ANALYSIS

There are two kinds of data available for the study of the adsorbed helium film. In raw form these consist of the heat capacity of the experimental cell and the pressure of the gas in the cell, both of these as a function of the temperature and of the amount of helium in the cell (a third kind of data, the heat of adsorption, is difficult to obtain in equilibrium except at high pressures; it will be shown below to be redundant). From these data we wish to extract the thermodynamic behavior of the film alone, and we wish to do so in a way that depends on as few assumptions as possible.

In principle, the pressure data alone are sufficient to give the complete thermodynamic behavior of the film. The pressure can be used to deduce the chemical potential of the film as a function of temperature and coverage, and from that all other thermodynamic properties follow. In practice, however, the pressure is too low to be measured for much of the range of temperature and coverage of most interest to us.

On the other hand, heat-capacity data from one cell alone are not sufficient to characterize the film thermodynamically, even in principle,[7] and moreover, the heat-capacity contribution of the film cannot be unambiguously extracted from the raw calorimetric data unless the pressure is either known or negligible. Thus it is clear that the two types of data are complementary. In this section we describe how to analyze the combined data in such a way as to produce a complete thermodynamic description of the film.

The thermodynamic analysis follows the terminology of Landau and Lifshitz[8] with modifications to better match the recommendations of the IUPAC.[9] The independent variables are taken as the chemical potential μ and the temperature T[10] because these are identical in all phases. The subscript "0" is used for extensive variables referring to all the helium in the experimental system. The subscript "g" is used for extensive variables referring to all the helium in a comparison system with the same free volume but negligible surface area. In practice this "comparison system" is just the bulk gas in the experimental system. The differences between the experimental system and the comparison system are called surface excesses and are not subscripted. The constants A and V and the intensive variables

μ, T, P, φ, and B do not need to be distinguished by subscripts.

Starting with the internal energy U_g of the comparison system, we may define in the usual way the Gibb's free energy

$$G_g = U_g - TS_g + PV \tag{1a}$$

and the Landau potential (the proper energy function of the grand canonical ensemble),

$$\Omega_g = U_g - TS_g - \mu N_g , \tag{1b}$$

so that

$$dU_g = T\,dS_g - P\,dV + \mu\,dN_g , \tag{2a}$$

$$dG_g = -S_g\,dT + V\,dP + \mu\,dN_g , \tag{2b}$$

$$d\Omega_g = -S_g\,dT - P\,dV - N_g\,d\mu . \tag{2c}$$

Since P depends on only μ and T, we may integrate (2c) at constant μ and T to get

$$\Omega_g = -PV . \tag{3}$$

If we now specialize to constant volume, we may drop dV and replace $V\,dP$ with $-d\Omega_g$ so (2) simplifies to

$$dU_g = T\,dS_g + \mu\,dN_g , \tag{4a}$$

$$dG_g = -S_g\,dT - d\Omega_g + \mu\,dN_g , \tag{4b}$$

$$d\Omega_g = -S_g\,dT - N_g\,d\mu . \tag{4c}$$

Also, from (1) and (3) we get

$$G_g = \mu N_g . \tag{4d}$$

Work of the PV kind has no meaning for the surface excess system, but its Landau potential is well defined by $\Omega = \Omega_0 - \Omega_g$. Thus, so long as no external work is done, equations like (4) can be written for all three systems. In particular, by replacing every subscript "g" in (4) by "0," we generate four more equations [to be referred to as Eqs. (5)], and dropping all subscripts gives another set of four [to be referred to as Eqs. (6)].

The experimental data may be converted into a complete thermodynamic description of the film as follows: From pressure isotherms at high temperature we may calculate $\mu(N_0)$ at constant T, using the formula from statistical mechanics[8]

$$\mu = kT \ln\left[\frac{P}{kT}\left(\frac{2\pi\hbar^2}{mkT}\right)^{3/2}\right] + BP ,$$

where B is the second virial coefficient, k is Boltzmann's constant, and m is the atomic mass. Explicitly, for ^{4}He with P in torr and μ in K,

$$\mu = T\ln(0.006419P/T^{2.5}) + (0.00033 - 0.0067/T)P .$$

We then find Ω_0 by integrating (5c) to get the Gibbs-Bangham equation[11]

$$\Omega_0 = -\int_{N_0=0}^{N_0} N_0\,d\mu \quad (T \text{ const}) .$$

Using (5b) and (5d) we find the entropy at a temperature midway between two isotherms by

$$S_0 = -\left(\frac{\partial\Omega_0}{\partial T}\right)_{N_0} - N_0\left(\frac{\partial\mu}{\partial T}\right)_{N_0} .$$

From the gross heat capacity of the calorimeter, we may find $C_0 = (\partial U_0/\partial T)_{N_0}$ by subtracting the calorimeter background, which is the gross heat capacity when $N_0 = 0$. We then have from (5a) that

$$C_0 = T\left(\frac{\partial S_0}{\partial T}\right)_{N_0} . \tag{7}$$

The entropy at the upper (+) and lower (−) isotherm is then

$$S_0 = -\left(\frac{\partial\Omega_0}{\partial T}\right)_{N_0} - N_0\left(\frac{\partial\mu}{\partial T}\right)_{N_0} \pm \frac{C_0\Delta T}{2\overline{T}} .$$

Thus we can find the function Ω_0, its proper variables T and μ, and its proper first derivatives $-S_0$ and $-N_0$, at each experimental point on a rectangular N_0, T grid. We may extend S_0 to lower temperatures, where the pressure is unmeasurably small at low coverage, by integrating (7). Equating the crossed second derivatives of $(G_0 + \Omega_0)$ with respect to T and N_0 and using (5b) gives the Maxwell relation

$$-\left(\frac{\partial\mu}{\partial T}\right)_{N_0} = \left(\frac{\partial S_0}{\partial N}\right)_T , \tag{8}$$

which allows us to calculate the chemical potential at lower temperatures, given the entropies at adjacent coverages. Then, using (5c) we may extend Ω_0 along an isostere. Finally, if it is possible to obtain heat-capacity data to low-enough temperatures to integrate S_0 accurately from absolute zero, the accuracy of the entire analysis increases by an order of magnitude because both proper derivatives of Ω_0 are then found by integrations rather than by differentiation. The accuracy at high coverage is also improved if the integration of Ω_0 is carried out along a series of isotherm and isostere segments such that N_g is always small along the isostere segments.

One simply subtracts Ω_g, N_g, and S_g from Ω_0, N_0, and S_0 to find Ω, N, and S respectively. For the current case where the comparison system is a dilute gas,

$$kTN_g = PV(1 - PB/kT) , \tag{9a}$$

$$S_g = 2.5N_g k + N_g k \ln\left[\frac{V}{N_g}\left(\frac{mkT}{2\pi\hbar^2}\right)^{3/2}\right] - \frac{N_g^2 k}{V}\left(B + T\frac{dB}{dT}\right). \tag{9b}$$

The data may now be used to deduce any other thermodynamic quantity of interest; for example[12]

$$q_{st} = 2.5kT + T(\partial\mu/\partial T)_N - \mu + N_g kT(B - TdB/dT)/V, \tag{10a}$$

$$q_d = 1.5kT + T(\partial\mu/\partial T)_N - \mu - 2N_g kT^2(dB/dT)/V, \tag{10b}$$

$$C_\phi = C + T[S/N - (\partial S/\partial N)_T](\partial\Omega/\partial T)_N/(\partial\Omega/\partial N)_T, \tag{10c}$$

where q_d is the differential heat of adsorption, q_{st} the isosteric heat of adsorption, and C_ϕ the heat capacity at constant two-dimensional spreading pressure, $\phi = -\Omega/A$; A is the substrate area.

By means of the techniques just described, raw data in the form of vapor pressures and gross heat capacities may be analyzed into a detailed and complete thermodynamic description of the adsorbed film. If the grid of data points is sufficiently complete, any desired thermodynamic property may be extracted. For example, as we shall see in Sec. IV, pressure isotherms may be constructed even at coverages and temperatures where direct pressure measurement is impossible. In any single experimental cell, the entire analysis may be done without recourse to any assumptions whatever about the microscopic nature or behavior of the adsorption system.

IV. DATA

The Caltech data resulted in the tabulation of over 4000 items between 4.5 and 15 K after analyzing with the methods of the preceding section. These are available[13] but are of limited utility in isolation because many of the interesting regions of the film occur below 4.5 K. Because considerable heat-capacity data are already available below 4.2 K, and the pressure was too small to measure, it was planned to use preexisting data from BDHMV to extend the analysis to lower temperatures.

While the data from a single cell could be analyzed without any reference to the surface area, the use of several cells required a normalization procedure. In principle, any distinctive feature could be used. For example, a traditional method is to find a break in a pressure isotherm using a nitrogen adsorbate at liquid-nitrogen temperature.[14] However, the optimal feature would be sharp and occur at a unique coverage and temperature so that the coverage calibration is not affected by small differences in the calibration of the temperature or other properties. Such a feature is provided by the triangular-lattice-gas ordering transition, where the helium has been shown to form an ordered state in registry with the graphite substrate.[15]

Heat capacities in the vicinity of this transition are shown in Fig. 1. An important bonus derived from calibrating with this feature is that absolute as well as relative areas may be determined. Since the size of the carbon lattice sites are well known, the coverage at the center of the transition can be determined to be $1/a = 6.366$ atoms/nm^2 (or $a = 15.71$ Å^2/atom). Data for three coverages are shown, using four cells from both BDHMV and Caltech. The feature is seen to vary rapidly with both temperature and coverage and to reproduce well in the different cells. Similar consistency was found at higher coverages.

Data from Caltech and BDHMV were combined to create Fig. 2. At the higher temperatures, the data were corrected for desorption using the surface excess formalism. The curves are con-

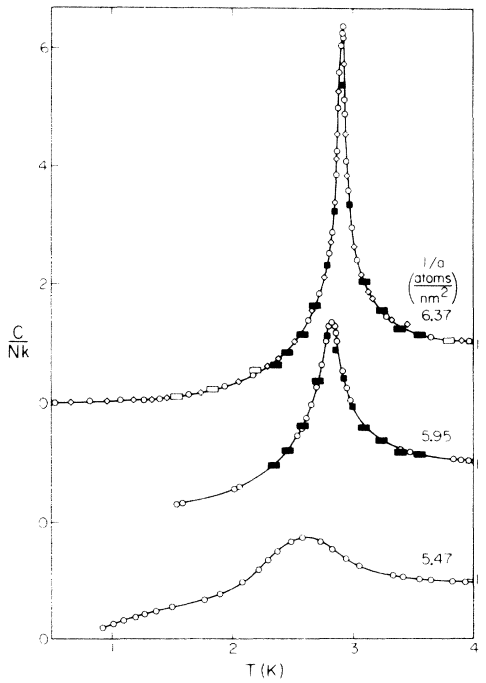

FIG. 1. Specific heat in the vicinity of the lattice-gas ordering transition. All coverages reported in this paper are normalized by assuming that the uppermost peaks occurs at 6.37 atoms/nm^2, corresponding to one helium atom for every six carbon atoms in the surface plane of the substrate. The circles and diamonds are data from two cells used by the BDHMV group; the open and filled boxes are from two cells used at Caltech.

tours connecting points of equal specific heat in the coverage-temperature plane. The intervals between heavy lines correspond to Boltzmann's constant. The intervals between light lines are 20% as large and dashed lines show 10% intervals where appropriate. Most of the data on which the region below 5 atoms/nm^2 and 2 K are based were taken before the importance of careful annealing (see Sec. II) was recognized. A peak earlier reported[16] at 5 atoms/nm^2 and 3 K may be identified as a ghost of the ordering peak caused by poor annealing; future measurements at lower coverage may sharpen the remaining low-coverage peak and strengthen the coverage dependence. The remainder of the figure should be accurate to a few percent with the following exceptions: Near 8 atoms/nm^2 and below 3 K the experimental data are too sparse for accurate interpolation. Below 0.5 atoms/nm^2 the accuracy is typically 10% because of the large calorimeter background. Above the diagonal line for which the coverage plus the temperature sums to 18, large desorption corrections also increase the uncertainty to 10% and more.

General features of film behavior can be identified for later discussion. The central region with a heat capacity slightly below 1.0 is a nearly ideal 2D gas. The lattice gas ordering transition

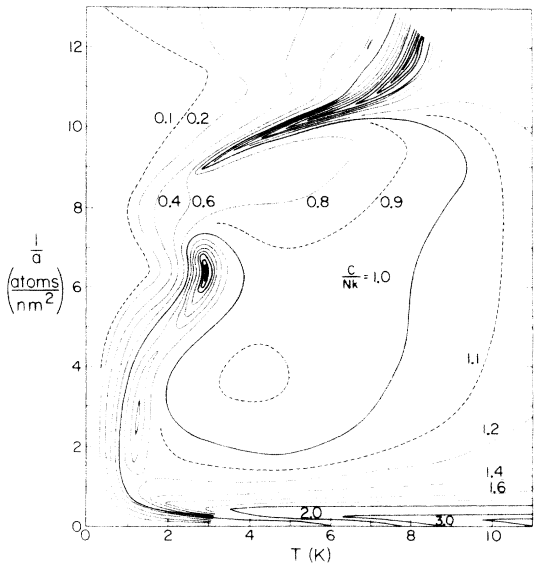

FIG. 2. Contours of constant specific heat in the coverage-temperature plane. Combined BDHMV and Caltech data are used, thermodynamically corrected for desorption. The heavy lines represent integral multiples of Boltzmann's constant; the lighter lines show 20% intervals between these, and the dashed lines 10% intervals where appropriate. The various topographical features are discussed in the text.

used for the area calibration is at $N = 6.366$ atoms/nm^2 and $T = 2.93$ K. The heat capacity rises slightly above 1.0 on the far right owing to occupation of single-particle excited states in the direction perpendicular to the surface. The ridge near the top is the melting transition. Above it is a 2D solid and second layer formation. The region between the melting transition and the ordered lattice gas is a dense fluid. The gentle peak rising above 1.6 at the lower left is called Bose compressed for lack of a better understanding. The region below 1 atom/nm^2 is dominated by inhomogeneities in the substrate.

The data are presented in the form of pressure isotherms in Fig. 3. In contrast to the heat capacity, which scarcely ranged over a factor of 10 in the region studied, the pressure variation is very large. It was found necessary to include a factor of T in addition to taking the logarithm in order to represent all the data in one graph. The full curves are pressure isotherms at 1.5 K temperature intervals. The dashed lines show the location of the ordering and melting transitions. The short curves give isotherms at 0.5 K intervals

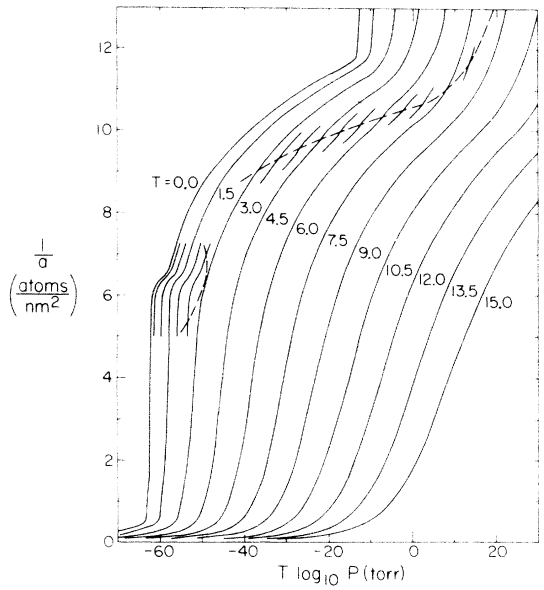

FIG. 3. Adsorption isotherms (curves of pressure vs coverage at constant temperature). The abscissa is represented in the form $T \log P$ in order to fit many orders of magnitude of pressure on the same plot. The dashed curve above 9 atoms/nm^2 is the melting transition, the dashed curve near 6 atoms/nm^2 is the lattice-gas ordering transition. The short solid curves in the regions of these transitions show isotherms at 0.5 K intervals; the other temperatures are shown. Pressures above 10^{-2} torr are measured directly. Lower pressures are deduced thermodynamically using heat capacity data.

in these regions. The large heat-capacity peaks associated with these transitions have little effect on the pressure isotherms, which depend mainly on the binding energy and compressibility at 0 K. Because of this low sensitivity, the relatively large uncertainties in Fig. 2 are not reflected in Fig. 3. The accuracy of the isotherms in Fig. 3 ranges from 0.01% of full scale for $T\log_{10}P>0$ to 1% of full scale for $T=0$.

The advantages of deriving the pressure thermodynamically, even in regions where it could in principle be measured directly, are shown in Fig. 4. Over this smaller range it is possible to use the pressure directly for the horizontal axis, but otherwise the curves are merely a more complete set of those shown in Fig. 3. The circles are direct pressure measurements made with the capacitive manometer concurrently with the heat-capacity measurements. The crosses show measurements using a residual-gas analyzer (RGA) on a separate Grafoil cell[17] (the coverage was normalized using pressures higher than those shown). Above 10^{-2} torr the calculated curves are based almost solely on the measured pressures so the agreement is not surprising. The curves were extended to lower pressures using the heat-capacity data and the methods of Sec. III. The melting transition is too sharp to be represented well by

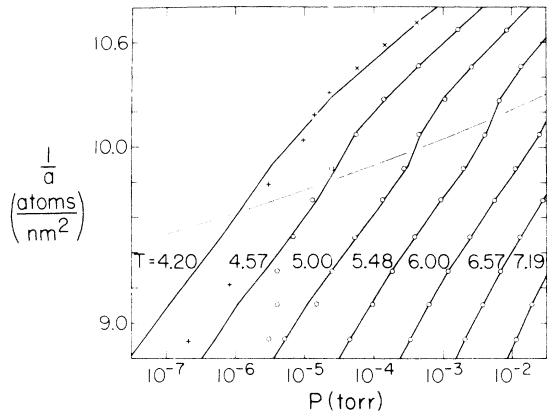

FIG. 4. Detail of the adsorption isotherms comparing directly measured pressures with deduced values. Open circles are pressures measured by room temperature capacitive manometry. Crosses show 4.2 K data in a different cell using a residual gas analyzer to measure pressure (coverage normalized at higher pressure than those shown). The heavy curves are based on the capacitive measurements above 10^{-2} torr, extended to lower pressures by means of heat-capacity data. The disagreement between these curves and the direct-pressure measurements at low pressures is attributed to the effects of incomplete equilibrium in the latter. The light curve shows the position of the melting transition.

the coarse data grid, but elsewhere the agreement remains excellent down to 3×10^{-5} torr. At lower pressures the deviations are within the $\pm3\times10^{-6}$ torr uncertainty (after thermal transpiration corrections) of the capacitive gauge. However, the RGA is capable of measuring below 10^{-9} torr and background contamination was equivalent to only 10^{-8} torr.[18] The factor of 5 disagreement for the lowest two points appears mainly owing to lack of complete equilibrium in the direct pressure measurements, even though each of these points took several days. The property that the lowest measured points show relatively little change in pressure with coverage is very common in the literature,[19] but apparently it is an artifact. The method used here is an improvement in two ways. High temperature annealing gives much faster equilibrium than any isothermal method and the heat capacity is much less sensitive than the directly measured pressure to the tendency of the film to be thickest nearest the inlet tube.

From the data incorporated in Figs. 2 and 3 we may derive the other thermodynamic functions using the methods of Sec. III. Specific applications will be given in the following sections. One particular application relates to the quality of the data itself. The entropy may be found either by integrating the data of Figs. 1 and 2 from 0 K or by integrating the data in Fig. 3 from 0 atoms/nm^2. These two methods generally agree within 2%, providing additional evidence that the adopted data are consistent and represent true equilibrium.

V. MODELING OF FILM

In Sec. III we showed how the thermodynamic behavior of the adsorbed film may be isolated from the raw data for the experimental cell as a whole. In this section we wish to show how the film data in turn may be decomposed into contributions from various distinct phenomena. In previous helium adsorption studies,[19] substrate inhomogeneity caused the measured heat capacity in most instances to be an admixture of contributions from parts of the helium film at various densities, behaving in different ways, and impossible to disentangle. In the ^{4}He-Grafoil system, however, the inhomogeneity is much smaller and better defined. Consequently, the various aspects of the behavior of the film are able to stand out more clearly, dominating the data in certain ranges of T and μ, and the result is that with some simple semiempirical modeling it is possible to sort out the contributions that go into much of the data.

As an example of how the procedure is to be carried out, consider the large central plain in

Fig. 2 where the specific heat stays in the range $0.9 < C/Nk < 1.1$. This is close to the behavior of a 2D ideal gas ($C = Nk$) and suggests that the small departures from ideality might be susceptible to correction by means of the virial equation of state. Siddon and Schick[20] have computed the quantum mechanical second virial coefficient for helium in 2D, and their results do in fact account for most of the departures from ideality in our data in the range $2 < 1/a < 5$ atoms/nm^2 and $1.5 < T < 7$ K.

In the same range of densities, but at higher temperature, the observed heat capacity rises above the virial equation predictions. We believe the excess heat capacity to be due to the excitation of single-particle excited states in the direction perpendicular to the substrate. These states were discussed by Jackson.[21] If the excitation energy for an atom is E_1, then these states contribute an energy per atom $E_1/(1+e^{E_1/kT})$ everywhere in the first layer, and an excess heat capacity

$$C^* = Nk\left(\frac{E_1}{2kT}\right)^2 \operatorname{sech}^2\left(\frac{E_1}{2kT}\right). \tag{11}$$

In Fig. 5 the excess heat capacity above the virial gas contribution is plotted in comparison to this function for two values of E_1. Data from seven coverages spanning 4 to 7 atoms/nm^2 were used. The excited-state energy E_1/k is thus determined to be 54 K above the ground state. When this contribution is added to the Siddon and Schick calculation, the range of agreement with the data is extended up to 15 K in temperature, and up to 8 atoms/nm^2 in coverage at the higher temperatures.

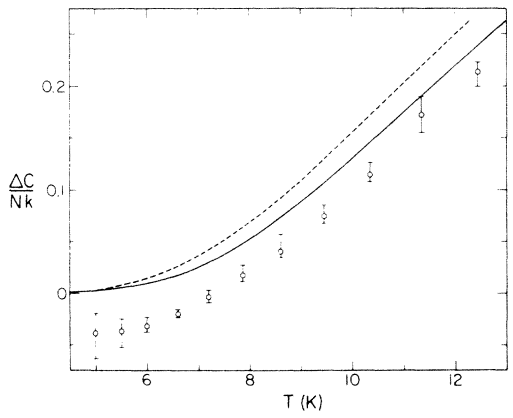

FIG. 5. Heat capacity due to a single-particle excited state perpendicular to the surface. Circles show the average excess heat capacity after quantum virial gas contribution has been subtracted. A monotonic dependence on coverage, from 4 to 7 atoms/nm^2, is shown by the error bars. This dependence, as well as the downward displacement of all the points, is probably due to the effects of substrate inhomogeneity not yet taken into account in this plot. The dashed and solid curves shown the function given in Eq. (11) for, respectively, $E_1/k = 52$ and 55 K.

C^* is part of the heat capacity for all N and T in the first layer, but it was necessary to find a region where C^* is appreciable and the rest of C well known in order to isolate it and measure E_1. That kind of sorting out is the first step in disentangling the contributions to the film data. The sorting out by itself is not enough, however, because in most cases the interaction between different aspects of the film behavior is more complex than the simple additive effect of the excited states.

To illustrate the next stage of reduction, we consider the ridge in the upper part of Fig. 2 which we have referred to as the melting transition. In Fig. 6 we show heat-capacity data along the ridge taken from BDHMV. We see that a dramatic change occurs in the peaks for coverages above 10.5 atoms/nm^2. The peaks become much higher and narrower than they are at lower coverage. We have proposed a quantitative explanation of this change[22] which we outline here.

Study of the data between 9 and 10 atoms/nm^2 suggests that the ridge separates a 2D solid on the low T side from a 2D fluid (we will discuss the evidence for a 2D solid in Sec. VI). When the solid melts, it tries to expand, as do many solids in 3D. Below 10 atoms/nm^2 the available area is constant, and so instead of expanding the transition causes the 2D spreading pressure ϕ to increase. However, at about 10.5 atoms/nm^2, the second layer starts to become populated. At this point the medium is able to expand by squeezing atoms out of the first layer into the second (and into the 3D gas as well). That process requires heat, owing to the difference in binding energy between the first and second layers (and the gas), and hence appears as an addition to the heat capacity. This has the effect of amplifying the underlying peak owing to melting in the first layer.

To make the model quantitative, we consider equilibrium between three subsystems: the first layer, the second layer, and the gas. The gas is a 3D ideal gas. The second layer is a 2D ideal gas with a binding energy of −30 K relative to the 3D gas (the second layer binding energy is deduced from the 0 K isotherm in Fig. 3). For the first layer we assume that its behavior after the second layer starts to form is the same as it is without the second layer. Its equation of state is therefore extrapolated by means of analytic forms fitted to the data below 10 atoms/nm^2. In equilibrium the three subsystems must have the

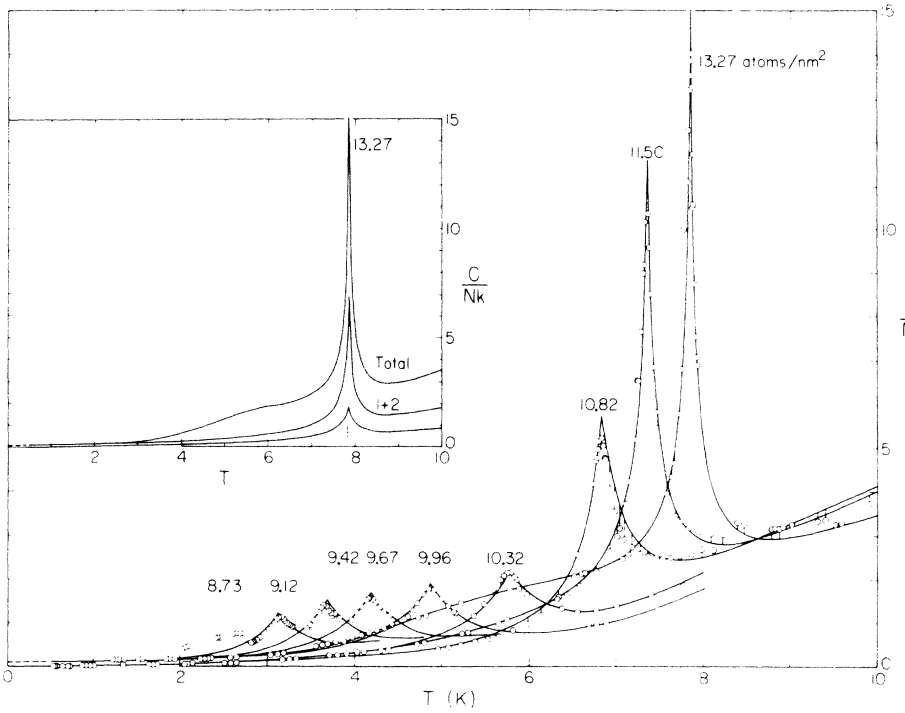

FIG. 6. Heat capacities near melting. All data points taken from BDHMV. All curves generated by the semiempirical model described in the text. Coverages are shown for each peak. In the inset the peak at 13.27 atoms/nm^2 is decomposed into contributions from melting in the first layer, promotion into the second layer, and desorption into the gas. Note especially the shoulder to the left of the peak, which is accounted for by the model.

same chemical potential, and the number of atoms in each is allowed to adjust itself subject to the constraint that the total N_0 is fixed. From the outcome, the heat capacity of the system may be computed, and the results are shown as the solid curves in Fig. 6.

Details of the parameters and analytic forms used to represent the first layer may be found in Ref. 22. There is relatively little room for maneuver in adjusting the parameters to fit the data. For example, the shapes of the large peaks could not be adjusted independently of the positions of their centers and the shapes of the smaller peaks. Nevertheless, the curves go right through the experimental data. In the inset of Fig. 6 we see one of the large peaks decomposed into contributions from the underlying first layer, promotion into the second layer, and promotion into the gas. Notice that the shoulder in the data to the left of the peak is reproduced by the model, although no attempt was made to do so. We also note *a posteriori* that promotion of atoms out of the first layer reduces the density in that layer, and has the effect of narrowing the transition, thus accounting for the fact that the peaks become narrower above 10.5 atoms/nm^2.

We believe that the success of this model justifies our use later on of first layer only data for further analysis, even when it comes from regions where higher layers have begun to form.

The essential principles we have just used to separate out the effects of second-layer formation will now be applied to isolate the influence of substrate inhomogeneity. The method is similar to that proposed by Ross[23]: to use the equation of state of an idealized film together with a binding energy distribution to produce the behavior of a real experimental film. Following Ross, we shall call the procedure the Ross-Olivier model.

Even a small amount of substrate inhomogeneity causes major effects at low coverage because the helium is preferentially adsorbed at the most energetic (least typical) sites. On the other hand, at high coverage the compressibility falls rapidly and the data are comparable to that expected on a uniform substrate with the same average binding energy. We may therefore use the experimental data with any multiple layers removed to represent an idealized film at high coverage. Below 5 atoms/nm^2 we use the virial gas equation of Siddon and Schick.[20] We now consider equilibrium among a continuum of subsystems each with a slightly different binding energy. Given the temperature and the chemical potential, the density appropriate to each binding energy is determined by the equation of state. We may calculate the pressure from μ and T and from the binding energy distribution function we may determine the average coverage and compare the results with Fig. 3.

Reversing this process to find the distribution function is usually very difficult. However, for the 0 K isotherm, energy variations due to the equation of state are negligible below 5 atoms/nm^2,

while binding energy effects are negligible above 1 atom/nm^2. This makes an iterative solution converge rapidly. In first approximation the binding energy is identical to the chemical potential at low coverage, with approximately 10 sites/nm.^{2} If θ is the fraction of the surface binding more strongly than E, the iterative solution is $E = -143[1 + (1 + \theta/0.026)^{-3}]$. Differentiating gives the distribution function $f(E) = 0.045(E + 143)^{-4/3}$, $143.0025 < -E < 286$, with E in K.

This functional dependence is very different from the Ross-Olivier Gaussian distribution but it may be derived from a simple model. If two surfaces make contact at a small angle, an atom in the corner is simultaneously adsorbed on both surfaces and will have twice the binding energy. The van der Waals's nature of the forces will cause the excess binding energy to vary as the inverse cube of the distance from the contact line. This model predicts that the surface area available to the second layer will be decreased by $2 \times 0.026 \times 100\% = 5.2\%$ owing to the filling of these corners. The 0.026 is a fit to data (see formula for E above), accuracy about 10%. This prediction is consistent with recent multilayer data.[24]

An example of the success of this model in explaining the low-coverage data is shown in Fig. 7.

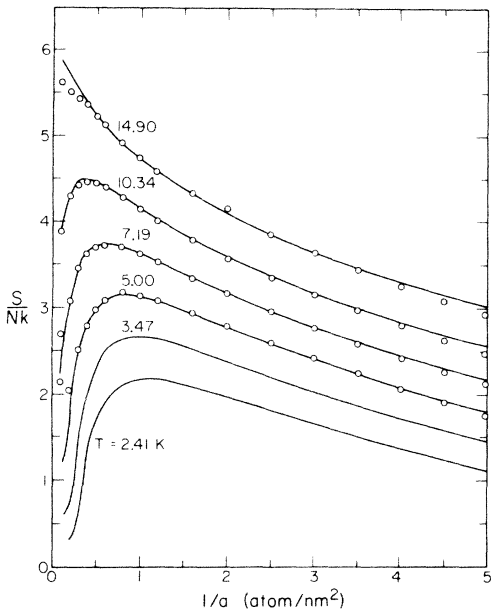

FIG. 7. Entropy-coverage isotherms in the low-coverage region. The temperature of each isotherm is shown in the figure. The points are measured values and the curves are generated from the semiempirical model discussed in the text. As low coverage is approached, the entropy rises logarithmically as a quantum virial gas, but this tendency is counterbalanced by the effect of substrate inhomogeneities.

The points give the experimental entropies calculated from the data in Figs. 2 and 3. The curves have been calculated from the preceding model. In the absence of inhomogeneity all the curves would show an identical logarithmic rise as the coverage falls if the virial gas behavior were to continue. In fact, we see that the entropy is strongly depressed, especially at low temperatures. The large heat capacities at the bottom of Fig. 2 are therefore due to a process akin to 2D desorption from the tight-binding sites. Good agreement is also found with the pressure isotherms in Fig. 3.

Both the ground-state and first-excited-state energies found here differ considerably from the predictions by Hagen, Novaco, and Milford[25] (-143 ± 2 and -89 ± 3 vs -188.8 and $\simeq -105$ predicted). Novaco[26] has recently noted that such discrepancies are within the uncertainties of the carbon-helium potential.

To recapitulate, the 2D helium film is accurately described by Siddon and Schick's virial gas predictions[20] above 4 K and below 7 atoms/nm^2. The deviations observed experimentally have been explained quantitatively in terms of a single-particle excited state and substrate inhomogeneity. At higher coverage similar analysis techniques allow us to separate out the contributions to the data from first-layer behavior and second-layer formation.

In all of the literature on physical adsorption, one of the most persistently recurring themes is the problem of identifying the point of monolayer completion. In the above model system the point of monolayer completion was uniquely defined by the first atom to enter the second layer. At finite temperatures or in the presence of substrate inhomogeneity, completion may occur at different points depending on the criterion used to define it. The melting model gives us enough information to compare and analyze the various theoretical and experimental criteria found in the literature.

The two most common experimental methods, the Langmuir and the B. E. T. isotherms,[14] give meaningless results at sufficiently low temperatures since the pressure varies exponentially with coverage. This exponential variation occurs when either the inhomogeneity energy or the interparticle interaction energies become large compared to the temperature, as is the case over the entire temperature range of the present experiment.

Jura and Hill[27] in connection with heat of immersion studies suggested the entropy minimum as a sounder criterion for monolayer completion. This criterion was also used by BDHMV by integrating their heat capacities from 0 K. It does not seem to have been noticed that essentially the same

criterion may be applied using only pressure isotherms near the monolayer. The trick is to plot the data in the form of a chemical potential versus the coverage. These lines will cross where the partial molar entropy is zero. The partial molar entropy is negative for a solid and positive for a gas, so every other crossing should indicate the completion of a layer.[28] When the lines cease crossing (or if they never cross), the 3D gas is no longer condensing into distinct layers. This monolayer criterion thus contains a built in test for homogeneity.[29] Plots of μ vs $1/a$ are shown in Fig. 8.

In the present case the second derivative of the chemical potential with density is positive for the 2D solid. This should be true for all other helium experiments, but it is not known whether it is true in general. When it is true, the point of inflection in a plot of μ vs T (or simply $\log P$ vs T) using a *single* isotherm will indicate the monolayer. Both the inflection and crossing criteria give essentially the same monolayer capacities in the present experiment. This drops about 1% for each 1 K rise in T with an extra 4% drop on crossing the melting line. The simple theoretical criterion that the next atom added has an equal probability

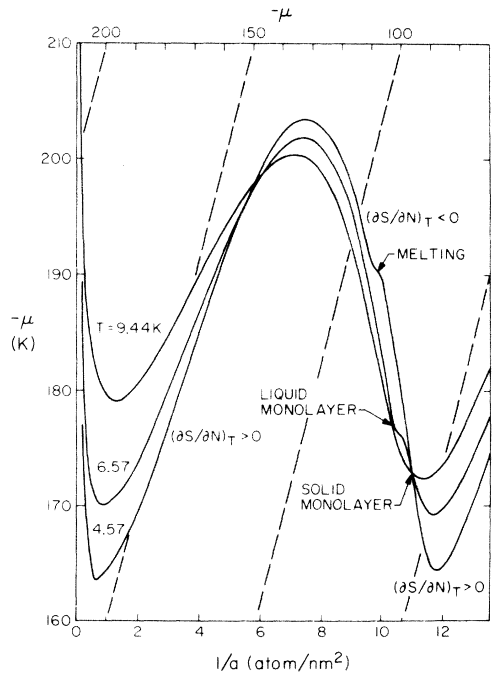

FIG. 8. Chemical potential-coverage isotherms. The vertical scale has been skewed, as shown by the dashed lines, to increase the sensitivity. Temperatures of the isotherms are shown. Various features, including regions of positive and negative partial molar entropy, are pointed out in the figure.

of going into either layer gives the same capacity at 0 K but only half the temperature dependence.

VI. SOLID STATE AND MELTING TRANSITION

In this section we wish to review the evidence that the upper left-hand region of Fig. 2 does in fact represent a 2D solid, and the ridge that bounds it represents a melting transition. We shall comment on the theoretical significance of these findings.

At low temperatures in 3D, the heat capacity of a solid is proportional to T^3 owing to the excitation of long-wavelength phonons. A 2D solid should, for the same reason, have a heat capacity proportional to T^2. This T^2 dependence for the heat capacity of near monolayer films has been reported for a number of systems,[30] and is found in Grafoil as well. In a study on argon coated copper, substitution of ^{3}He for ^{4}He at about the same density was shown to change the coefficient of the heat capacity in the ratio of 3:4,[31] further supporting the supposition that 2D phonons are responsible for the observations. However, the mere fact that phonons are excited is not enough to identify the 2D medium as a solid. It is necessary to show that both transverse and longitudinal modes are present. Thus, in 3D, liquid ^{4}He has a T^3 heat capacity at low T, but it is due to excitation of longitudinal phonons only.

In order to determine whether transverse modes are present it is necessary to have an independent measurement of the elastic properties of the medium. For this purpose we may use the two-dimensional compressibility K_2. Measurements of K_2 were first reported by Stewart, Siegel, and Goodstein.[17] Values in agreement with those may be extracted from our own data. The compressibility is given by

$$K_2 = -\frac{1}{a}\left(\frac{\partial a}{\partial \phi}\right) = -\frac{\partial a}{\partial \mu} \ . \tag{12}$$

If the medium is a fluid, supporting longitudinal sound waves only, then the Debye temperature should be directly related to the compressibility by

$$\theta_D^2 = \frac{8\pi\hbar^2}{mk^2 K_2} \ , \tag{13}$$

where the θ_D's are derived from the experimental heat capacities according to

$$C/Nk = 28.8(T/\theta_D)^2 \ . \tag{14}$$

Instead, the measured θ_D^2's are smaller than those predicted by Eq. (13) by a factor of 4 or more. To account for the difference, we must assume low-frequency transverse modes are present, in which

case

$$\theta_D = \frac{2\pi\hbar}{k}\left(\frac{N}{A}\right)^{1/2}\left(\frac{2}{\pi}\right)^{1/2}\left(\frac{1}{c_t^2}+\frac{1}{c_l^2}\right)^{-1/2}, \qquad (15)$$

where c_t and c_l are the transverse and longitudinal sound speeds. Since c_t must always be less than c_l, θ_D is dominated by the excitation of low-lying transverse modes, and is consequently considerably smaller than it would be in a medium with the same compressibility and only longitudinal modes.

As reported by Stewart *et al.*,[17] the compressibility and Debye temperatures together suffice to give the Poisson's ratio σ of the medium. For a fluid in 2D the Poisson's ratio is equal to 1; any lower value implies the existence of transverse modes. The measured value of σ for ^{4}He is between 0.6 and 0.7 over the entire zone we claim to be 2D solid. In 3D solid ^{4}He, the corresponding values are $\sigma = 0.5$ for fluid, $\sigma \cong 0.3$ observed. We thus have direct evidence that the medium supports transverse modes, or, in other words, that is resists shear stresses.

It should be noted that if the film were partially a uniform phase in registration with the substrate lattice, the melting peak and Poisson's ratio ought to show oscillations as the coverage varies through the values of optimum registration. Since no such variations were observed (the sharpening of the melting peak near 6 K has already been explained in terms of multilayer formation), the shear resistance is evidently intrinsic to the film.

The picture of an isotropic 2D solid is further supported by an analysis performed by Stewart.[32] Under certain specific conditions the two elastic constants of an isotropic medium are not independent, but are related instead by the Cauchy conditions. When this is true in either 2D or 3D, Poisson's ratio is fixed. In 3D the Cauchy conditions give $\sigma = 0.25$ in 2D, $\sigma = 0.33$ for any material obeying them. However, the ordinary Cauchy conditions need to be modified for helium, because helium does not form a solid under its own vapor pressure in 3D, nor at zero spreading pressure in 2D. When the Cauchy conditions are applied under conditions of initial stress, σ comes to depend on the applied pressure and the compressibility. Analyzing the situation in 3D, Stewart finds that the Cauchy conditions correctly predict σ and its dependence on density over the entire range of existing data for solid ^{4}He. In 2D the predicted value (using our data for the applied spreading pressure and compressibility at 0 K) is $\sigma \simeq 0.53$, reasonably close to the measured value of 0.6–0.7 quoted above.

Other evidence that the medium is a 2D solid has been quoted by BDHMV and is based on the striking similarity between certain properties of the film and the corresponding properties of 3D solid helium at the same interparticle spacing. For example, the Debye temperatures at the same interatomic spacings[33] are compared in Fig. 9. The circles are 2D and the crosses 3D. It should be possible to calculate a unique ratio between θ_2 and θ_3 for close packed crystals from elastic theory. Such a program has not been carried out, but the experimental ratio does appear to be independent of density. The melting temperatures at corresponding interatomic spacings are shown in Fig. 10. In 2D the two phases do not coexist at different densities as they do for the first order transition found in 3D. However, the heat-capacity peaks, shown by circles, are found at the same densities as the two-phase region shown for 3D. (The squares are a theoretical prediction, to be explained below.)

The melting peak in the heat capacity at constant 2D pressure C_ϕ is shown in Fig. 11 together with the nearby isosteric heat capacities from which it is deduced [see Eq. (10c)]. Although C_ϕ is obviously sharper than $C_{\rm exp}$, it is clearly not the δ function singularity one would expect if the transition were first order. With the complete thermodynamic description obtained in this project, we can go further and compare the entire equations of state. That is done in Fig. 12: There are striking similarities between the observed 2D behavior and 3D melting, but we see once again that the transition we are observing in 2D is not first order. Nevertheless, we are inclined to accept the identification of this phenomenon as the melting transition in 2D.

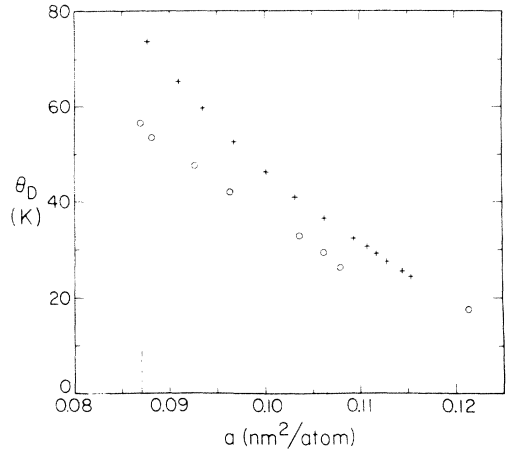

FIG. 9. Debye temperatures as a function of density. The circles are 2D values reported by BDHMV. The crosses are for 3D bulk hcp solid ^{4}He, scaled to an equivalent 2D density, as explained in Ref. 33.

There is a class of ordered states of matter which are not supposed to occur in 2D. The class includes superfluidity, superconductivity, and certain kinds of magnetic order.[34] In particular, the class also includes crystalline solids.[35] We wish to comment upon the relation between this theorem and the evidence we have reviewed above for the existence of a 2D solid.

Crystals as they are conventionally defined cannot exist in 2D because the mean-square thermal fluctuations in the position of an atom in the lattice would increase as the logarithm of the distance between the atom's lattice site and the origin. Thus at any finite temperature there cannot be a well-defined crystal lattice in the thermodynamic limit. The importance of this theorem is underscored by the apparent connection between these mean-square fluctuations and the melting of solids in 3D. If we suppose that solids melt when the thermal mean-square displacement of the atoms, δ^2, becomes equal to some fraction of the square of the lattice parameter a_0^2 the result is a melting temperature in agreement with empirical observation. In particular, assuming that melting occurs when

$$\delta^2/a_0^2=\gamma \ , \tag{16}$$

then the melting temperature of a 3D harmonic solid is then given by

$$T_m=\frac{\gamma}{2.19}\frac{mk}{8\hbar}a_0^2\theta_D^2 \ . \tag{17}$$

This result is in agreement with the Lindemann empirical melting formula,[36] which observes that solids melt when

$$T=C_L v^{2/3}\theta_D^2 \ , \tag{18}$$

where v is the molecular volume and C_L an empirical constant. Applying the same idea in 2D, the theorem above tells us that the melting temperature will always be 0 K, since δ^2 diverges in the thermodynamic limit at all finite temperatures.

Nevertheless, we shall argue here that the theorem is not in conflict with the evidence we have presented, and furthermore that the Lindemann formula may be derived from entirely different arguments which do not stress the role of the mean-square displacements.

It is clear that we have not and cannot present experimental proof that an infinite 2D crystal would exist in an ideal 2D world. The extent of the observed 2D solid may be limited by the size

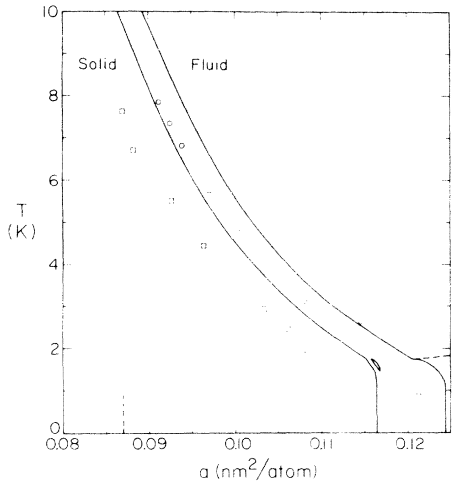

FIG. 10. Melting curve. Circles show the positions of the melting peaks (see Fig. 6) as a function of density in the first layer only, corrected from the raw data by means of the semiempirical model. The solid curves show the phase diagram of bulk helium scaled to 2D density by the same method used in Fig. 9. The squares are the predictions of the Kostlerlitz-Thouless-Feynman theory using 0 K Debye temperatures from BDHMV. The predicted temperatures are higher than those given by Eq. (21) by a factor 1.15, since that equation is for a square lattice, but we believe the real lattice to be tcp.

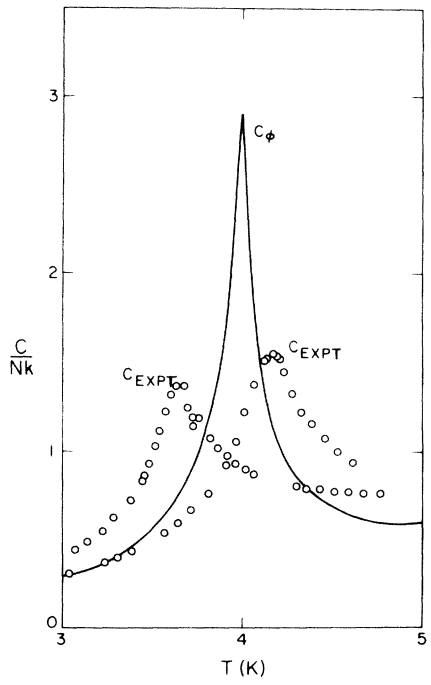

FIG. 11. Specific heat at the melting transition. The data points labeled C_{exp} show two of the peaks in the isosteric heat capacity attributed to melting in the first layer only. The curve shows C_ϕ, the specific heat at constant 2D pressure, generated by means of Eq. (10c). In a first-order phase transition, C_ϕ would appear as a δ-function infinity.

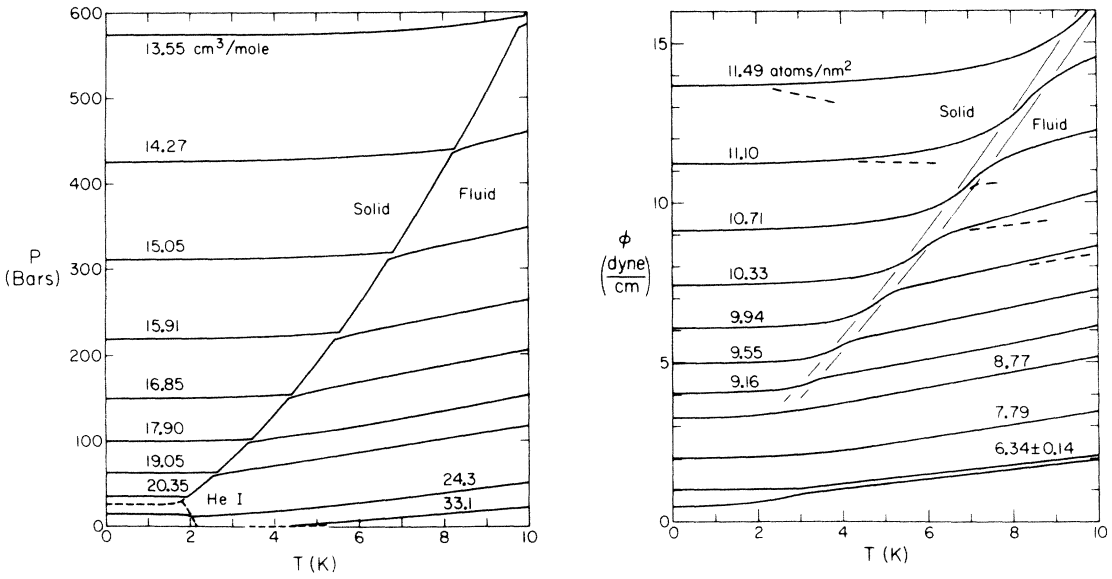

FIG. 12. Isochors through melting in the pressure-temperature plane. The left-hand figure, included for comparison, shows behavior in bulk ^{4}He with isochors at densities comparable to those in the 2D plot on the right-hand side (the 2D-3D scaling is the same as that used in Figs. 9 and 10). The right-hand figure has been corrected to first-layer-only data using the semiempirical model. The dashed lines show uncorrected isochors including the second layer (i.e., data with only desorption into the gas corrected for). On each isochor, the heat-capacity melting peak occurs at the point of maximum slope in the transition region. Along each isochor between the lighter curves, the medium undergoes a change in entropy of $\frac{1}{3}$ the entropy change observed in 3D melting.

of the Grafoil platelets, which is not well known.[1] Moreover, the structure of the film may be influenced by the crystalline substrate upon which it is adsorbed. As we have argued above, the close correspondence between the properties of the 2D and 3D solid ^{4}He seems to imply that the film in this range of μ and T is not much influenced by the substrate, but that argument is not conclusive. However, we do not believe that the nonideality of the experimental film is central to the question at hand. We wish to argue instead that the theorem does not preclude the existence even of an ideal infinite 2D solid with the properties we have attributed to the helium film.

The central observation which identifies the state in question as a 2D solid is the fact that it supports long-wavelength, low-frequency transverse sound waves. That observation means that it resists shear stresses. If we are able to demonstrate in 3D that a medium resists shear stress, we identify it as a solid. It may, to be sure, not be a crystalline solid; glasses and amorphous solids resist shear stresses as well. However, we believe we can rule out the possibility that the observed film is a 2D analog of a glass or amorphous solid. Amorphous materials are not equilibrium states of matter. If heated and annealed, they tend to crystallize or at least show hysteresis; moreover, if cooled to 0 K they have residual entropy. The experimental technique for studying the films, on the other hand, involved repeated warming and annealing, as described above in Sec. II. Furthermore, as mentioned in Sec. IV, the absolute entropy of the film has been measured both by integrating the heat capacity from 0 K at constant N, and by integrating the partial molar entropy from zero coverage at constant T. The agreement found between the results of these procedures indicate that the film entropy goes to zero at 0 K. We therefore believe that we are dealing with a state of matter which, in thermodynamic equilibrium, resists long-wavelength shear stresses. In 3D only crystalline solids have these properties.

Thus solidity (the ability to resist shear stress) and crystallinity (finite δ^2 about all sites in an infinite lattice) are always found together at equilibrium in 3D. Nevertheless, we know of no fundamental law which specifies that the former implies the latter. Instead, we may have in 2D a medium which has solidity, as observed, even though infinite-range crystallinity is forbidden. Such a 2D medium would still be an ordered state, with atoms in any local region falling on well-defined lattice sites. The spatial correlations between the positions of atoms are washed out at long distances owing to thermal fluctuations, but angular correlations between directions in the

lattice are preserved, even in the thermodynamic limit.[22] Such a medium could not have a sharp x-ray diffraction pattern (since the x-ray intensity is the Fourier transform of the spatial correlations) but it could have many other properties common to crystals in 3D, among them of course, shear resistance. The point of view we have just described has been adopted by Kosterlitz and Thouless,[37] and by Feynman,[38] who also present a theory of melting of 2D solids. An alternative view of the role of order and the melting phenomenon in 2D has been presented by Dash and Bretz.[39] We have previously reviewed and compared these theories,[22] and do not wish to do so again in detail here. However, we would like to point out again the relation between the Kosterlitz-Thouless-Feynman theory and the Lindemann formula cited above.

In the Kosterlitz-Thouless-Feynman view, melting in 2D is a consequence of the thermal excitation of dislocation pairs in the 2D solid. If the energy in the strain field of a dislocation pair is given by

$$E_p = 2L \ln(r/a_0), \tag{19}$$

where r is the distance between the members of the pair, then the solid melts at the temperature $T_m = L/k$, where the average value of r^2 diverges. Feynman has computed L for a 2D solid and gives for the result

$$L = \frac{m}{8\pi} \frac{c_t^2 c_l^2}{c_t^2 + c_l^2} \tag{20}$$

for a square lattice, where c_t and c_l are the speeds of sound as above. The speeds of sound enter into the 2D Debye temperature in this same combination, so the predicted melting temperature may be expressed as

$$T_m = \left(\frac{1}{2\pi}\right)^2 \frac{mk}{8\hbar^2} a_0^2 \theta_D^2 . \tag{21}$$

This has the same form as the Lindemann formula, Eq. (17) above, with the arbitrary constant γ replaced by $2.19/(2\pi)^2 \simeq \frac{1}{18}$, a value that is not unreasonable. The melting temperatures predicted by this theory are shown by the squares in Fig. 10. It must be remembered, of course, that the theory giving rise to Eq. (21) is not applicable in 3D where Eq. (17) is found to work, since dislocations are very much more complicated in 3D than in 2D. Nevertheless we feel that this result shows that the Lindemann formula cannot be used to establish a direct connection between the melting of a solid and the finiteness of δ^2. Thus, the argument we gave earlier in this section, indicating that 2D solids should melt at 0 K, loses its force.

VII. ORDERING PEAK AND LOWER DENSITIES

The general behavior of the film at densities below the ordering density is summarized by means of isotherms in a plot of φ vs $1/a$ (i.e., in the 2D pressure-density plane) in Fig. 13. The region below about 1 atom/nm^2 is dominated by inhomogeneities. Between 1 and 4 atoms/nm^2 the behavior is close to that of an ideal gas in 2D, with $\varphi \propto (1/a)T$. The sharp increase in slope to the right is due to the formation of the ordered lattice gas. Whatever phenomena are associated with the heat capacity peaks in the Bose compressed region occur between the 0 and 1.5 K isotherms, where there is insufficient data to resolve the equation of state.

Ideally, the behavior of the 2D film should be easiest to account for in the low-density limit, but in practice that is just where all observations are dominated by substrate inhomogeneities. Thus, for example, Widom and Sokoloff[40] have proposed a virial expansion by means of which the 2D interaction might have been deduced from the 3D gas pressures, but they assumed a spectrum of binding energies whose width is small compared to the temperature. Since the reverse is true at low 2D density, and their approxima-

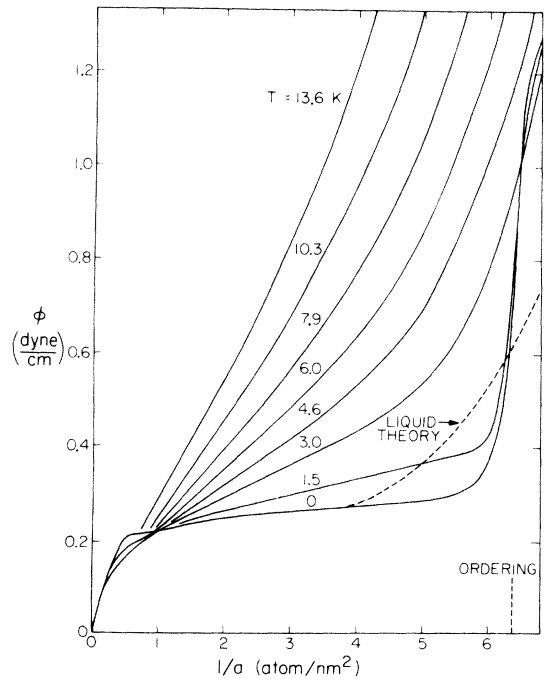

FIG. 13. Isotherms in the 2D pressure-density plane at low coverage. Temperatures are shown in the figure, as well as the ordering density and the behavior of a predicted liquid state discussed in the text.

tions are applicable only at low density, it is not surprising that the form they predict for the adsorption isotherms is never found to be applicable.

The behavior that actually is observed in the low-density limit of Fig. 13 is most easily described as a region of negative 2D pressure relative to an ideal homogeneous substrate. The negative pressure is applied by the inhomogeneities, which attract the helium away from the more ideal portion of the substrate. To a first approximation, the behavior of the film on an ideal substrate may be seen by shifting both axes to ignore the inhomogeneity dominated region.

Dash[41] has observed that the heat capacity at 0.5 atoms/nm^2 has the form of a 2D Debye solid up to 4 K, and has proposed the existence of a low-density solid region in that part of the phase diagram that we are calling inhomogeneity dominated. Our own data confirm this form all the way up to 15 K, but the agreement does not obtain at either higher or lower density. The heat capacity in this region is accounted for by the Ross-Oliver-type model discussed in Sec. V. The form is in fact due to the presence of 2D solid, but it is the ordinary high-density solid which forms on the inhomogeneous portions of the substrate.

The equation of state of a 0 K liquid, according to Miller, Woo, and Campbell[42] is shown by the dashed curve in Fig. 13. The data do not confirm the existence of such a state. Novaco[43] has estimated that the ordered lattice gas should be more stable than this liquid, but less stable than the 2D ideal gas. These predictions are confirmed by the observations at 1.5 K. If the ordered state were more stable than the gas, this isotherm would be horizontal, since patches of ordered state would form at low coverage, filling up the surface at constant ϕ as the coverage increases. Instead the ordered state becomes stable only at some sufficiently elevated 2D pressure.

It should be noted that the ordered state itself is characterized by a compressibility which apparently approaches zero. This is in sharp distinction to the behavior, say, at a gas-liquid critical point, where the compressibility diverges. The small compressibility is in excellent agreement with the picture that in this state the helium atoms are found on sites fixed by the rigid graphite substrate. The zeroing of the compressibility, which shows up as the sharp rise in ϕ on the right-hand side of Fig. 13 may also be seen in the 3D pressure isotherms in Fig. 3. There have been many reports of gas-liquid equilibrium in various films,[44] which are detected by means of a vertical portion on an adsorption isotherm. The lattice gas ordering phenomenon is characterized instead by a decrease in the slopes of the isotherms.

VIII. CONCLUSIONS

The general picture of the ^{4}He-Grafoil system that emerges from this study does not differ in any fundamental respect from that put forward earlier by BDHMV, but it has been enriched by the addition of many quantitative details. Broadly speaking, there is a 2D solid at low T and high N in the first layer, bounded by a melting transition. The fluid phase on the low-N high-T side of the transition may generally be described as a quantum virial gas, especially when the single-particle excited state perpendicular to the surface is taken into account. These phases and the transition between them seem little affected by the substrate potential once the semi-empirical models have been used to remove the effects of substrate inhomogeneity and of second-layer formation. The unimportance of the periodic potential found even on a perfect graphite substrate confirms estimates[25] that the helium zero-point energy is large compared to the barrier height between potential adsorption sites on the substrate. However, at a coverage corresponding to one helium atom for every three carbon hexagons in the graphite basal plane substrate, the substrate potential is able to "shine through" and impose upon the helium an ordered state in registry with itself. This latter phenomenon is observed as the lattice-gas ordering peak.

The particular contributions of this project to understanding the ^{4}He-Grafoil system arise from the new calorimetric and vapor-pressure data above 4 K, the combined thermodynamic analysis made possible by those data, and application of the technique of semiempirical modeling of the film. In addition, dependable criteria for ascertaining equilibrium in the film have been developed and, we believe, important new insights have been gained as a result of Feynman's interest in this work.

The analyses of the data that we have presented have allowed us to show that the dramatic increase in the heights of the melting peaks at elevated densities are a consequence of second-layer formation, and that the observed low-density heat capacities are due to the formation of compressed helium film on inhomogeneous portions of the substrate. The ground-state and first-excited-state energies of a helium atom adsorbed on a perfect Grafoil substrate have been measured to be -143 ± 2 and -89 ± 3 K, respectively. Earlier vapor-pressure measurements in this laboratory, confirmed in the present work, have given the 2D

compressibilities of the film; these together with Debye temperatures from BDHMV have made it possible to establish the presence of transverse sound modes in the solid phase. Moreover, isochores in the 2D pressure temperature plane have been constructed allowing detailed characterization of the melting transition. In the fluid region we have confirmed that the 2D ideal gas with quantum virial correction gives an accurate account of the system.

Finally, it should be pointed out that the studies of the kind we have reported here may be expected to lead to new insights into the nature of matter in 3D. As an example, Stewart's study of the elastic properties of the 2D medium has led to the observation, evidently not previously realized, that the Debye temperature of 3D solid ^{4}He are consistent with the Cauchy conditions if initial stress is properly taken into account. More speculative but perhaps more fundamental is the discovery that the 2D dislocation theory of melting gives rise to the 3D Lindemann empirical melting formula. In a similar vein, we see in the 2D solid for the first time clear evidence for a material which, in its equilibrium state, resists low-frequency shear stresses, but cannot have the spatial correlations usually associated with crystallinity. Moreover, when the 2D solid melts, the transition is not first order, although melting in 3D is always first order. This observation tends to lend weight to the view[45] that melting in 3D must always be first order because the long-range spatial order of 3D crystals is a property that cannot vanish in a continuous way.

ACKNOWLEDGMENTS

The authors owe a substantial debt of gratitude to Professor R. P. Feynman, not only for the very real, direct contributions he has made to this work, but also for his continuing enthusiasm and support. We are also indebted to Professor J. G. Dash, the other members of BDHMV, and the rest of the Seattle group for their generous sharing of data and ideas. Professor G. A. Stewart has materially aided the progress of this work, and we are grateful to him and to Jeffrey Greif for countless discussions and contributions.

---

*Supported in part under NSF Grant No. GH34682.

†Present address: 26-147 MIT, Cambridge, Mass. 02139.

[1]M. Bretz, J. G. Dash, D. C. Hickernell, E. O. McLean, and O. E. Vilches, Phys. Rev. A 8, 1589 (1973).

[2]GTA grade Grafoil ®, produced by Union Carbide.

[3]J. G. Dash and J. Siegwarth, Rev. Sci. Instrum. 34, 1276 (1963).

[4]For further details concerning the apparatus see R. L. Elgin, thesis (California Institute of Technology, 1973), unpublished (available from University Microfilms, Ann Arbor).

[5]T. Edmonds and J. P. Hobson, J. Vac. Sci. Technol. 2, 182 (1965); J. P. Hobson, J. Vac. Sci. Technol. 6, 257 (1969); J. Vac. Sci. Technol. 7, 351 (1970); G. T. McConville, Cryogenics 9, 122 (1969); R. A. Watkins, W. L. Taylor, and W. J. Hanbach, J. Chem. Phys. 46, 1007 (1967); J. Chem. Phys. 47, erratum 3692.

[6]S. W. Weber, W. H. Keesom, and G. Schmidt, Commun. Kamerlingh Onnes Lab. Univ. Leiden No. 246a (1937); see also Nos. 223b Suppl. (1932), 716 (1933), and 246b, c, d (1937).

[7]It is possible in principle to deduce the vapor pressure from heat capacities if measurements are made in two cells with different free volumes. See J. G. Dash, R. E. Peierls, and G. A. Stewart, Phys. Rev. A 2, 932 (1970).

[8]L. D. Landau and E. M. Lifshitz, *Statistical Physics*, 2nd ed., translated by J. B. Sykes and M. J. Kearsley (Addison Wesley, Reading, Mass., 1969).

[9]M. L. McGlashan, J. Chem. Educ. 43, 226 (1966).

[10]A. Widom, Phys. Rev. 185, 344 (1969).

[11]T. L. Hill, J. Chem. Phys. 17, 520 (1949).

[12]Ref. 4, pp. 42–51.

[13]See Ref. 4, Appendix I.

[14]See, for example, D. M. Young and A. D. Crowell, *Physical Adsorption of Gases* (Butterworths, London, 1962).

[15]M. Bretz and J. G. Dash, Phys. Rev. Lett. 28, 729 (1972).

[16]See Ref. 1, particularly Fig. 19.

[17]G. A. Stewart, S. Siegel, and D. L. Goodstein, in *Proceedings of the 13th International Conference on Low Temperature Physics, Boulder, Colorado, 1972* (Plenum, New York, to be published).

[18]J. L. Wallace and D. L. Goodstein, J. Low Temp. Phys. 3, 283 (1970).

[19]See, for example, W. D. McCormick, D. L. Goodstein, and J. G. Dash, Phys. Rev. 168, 249 (1968).

[20]R. L. Siddon and M. Schick, Phys. Rev. A 9, 907 (1974); in *Monolayer and Submonolayer Films*, edited by J. G. Daunt and E. Lerner (Plenum, New York, 1973), pp. 65–74.

[21]H. W. Jackson, Phys. Rev. 180, 184 (1969).

[22]R. L. Elgin and D. L. Goodstein, in *Monolayer and Submonolayer Films*, edited by J. G. Daunt and E. Lerner (Plenum, New York, 1973), pp. 35–52.

[23]S. Ross, in *The Solid-Gas Interface*, edited by E. A. Flood (Dekker, New York, 1966).

[24]Data in the multilayer region and in the monolayer region using ^{3}He are being analyzed and will be presented in a later publication.

[25]D. E. Hagen, A. D. Novaco, and F. J. Milford, *Proceedings of the 2nd International Symposium on Adsorption-Desorption Phenomena, Florence, Italy, 1971* (Academic, New York, 1972).

[26]A. D. Novaco, Phys. Rev. A 7, 1653 (1973).
[27]G. Jura and T. L. Hill, J. Am. Chem. Soc. 74, 1598 (1952).
[28]The other crossings indicate the transition from dilute to dense fluid within a single layer. Below the critical temperature, plotting $T\log(P_0/P)$, where P_0 is the vapor pressure in the bulk, should give the more sensitive test of whether the partial entropy is above the bulk value.
[29]An experiment in this laboratory using helium on oxidized copper gave no crossings for $T > 4$ K.
[30]H. P. R. Frederickse, Physica 15, 860 (1949) [the significance of the T^2 dependence in these measurements was pointed out by W. Band, Phys. Rev. 76, 441 (1949)]; W. D. McCormick *et al.*, Ref. 19; D. F. Brewer, A. J. Symonds, and A. L. Thomson, Phys. Rev. Lett. 15, 182 (1965); G. A. Stewart and J. G. Dash, Phys. Rev. A 2, 918 (1970); J. Low Temp. Phys. 5, 1 (1971). See also J. G. Dash, J. Low Temp. Phys. 1, 173 (1969).
[31]D. L. Goodstein, W. D. McCormick, and J. G. Dash, Phys. Rev. Lett. 15, 447 (1965).
[32]G. A. Stewart, Phys. Rev. A (to be published).
[33]Solid ^{4}He in 3D is hexagonal close packed (hcp) at 0 K. The close packed 2D structure is triangular (tcp). The atomic area that corresponds to the same interatomic spacing at a given volume for these crystals is $a = 1.091v^{2/3}$. This scaling was used in Figs. 9, 10, and 12.
[34]P. C. Hohenberg, Phys. Rev. 158, 383 (1967).
[35]See Ref. 34. See also R. E. Peierls, Ann. Inst. Henri Poincare 5, 177 (1935); L. D. Landau, Phys. Z. Sowjetunion 11, 26 (1937); B. Jancovici, Phys. Rev. Lett. 19, 20 (1967); L. Gunther, Phys. Lett. 25A, 649 (1967); 26A, errata (1968); N. D. Mermin, Phys. Rev. 176, 250 (1968); Y. Imry and L. Gunther, Phys. Rev. B 3, 3939 (1970); J. F. Fernandez, Phys. Rev. A 2, 2555 (1970).
[36]F. A. Lindemann, Z. Physik 11, 609 (1910).
[37]J. M. Kosterlitz and D. J. Thouless, J. Phys. C 5, L124 (1972); J. Phys. C 6, 1181 (1973).
[38]R. P. Feynman, as reported in Ref. 22.
[39]J. G. Dash and M. Bretz, J. Low Temp. Phys. 9, 291 (1972).
[40]A. Widom and J. B. Sokoloff, Phys. Rev. A 5, 475 (1972).
[41]J. G. Dash, in Ref. 17.
[42]M. D. Miller, C. W. Woo, and C. E. Campbell, Phys. Rev. A 6, 1942 (1972).
[43]See Ref. 26.
[44]A number of such reports are reviewed in Ref. 14. See also A. Thomy and X. Duval, J. Chim. Phys. Physiocochim. Biol. 66, 1966 (1969); J. Chim. Phys. Physiocochim. Biol. 67, 286 (1970); J. Chim. Phys. Physiocochim. Biol. 67, 1101 (1970).
[45]See Ref. 8, p. 264.